A robustness-enhanced method for Riemann solver

Shaolong Guo, Wen-Quan Tao

A robustness-enhanced method for Riemann solver

Shaolong Guo[a,b], Wen-Quan Tao[a,*]

[a] Key Laboratory of Thermo-fluid Science and Engineering of MOE, School of Energy & Power Engineering, Xi'an Jiaotong University, Xi'an 710049, China
[b] Aix Marseille Univ, CNRS, Centrale Marseille, Marseille, M2P2, France

ARTICLE INFO

Article history:
Received 20 August 2020
Revised 12 November 2020
Accepted 24 November 2020
Available online 3 December 2020

Keywords:
Carbuncle phenomenon
Shock instability
Flux splitting
Low diffusion

ABSTRACT

The appearance of shock anomaly is a major unsolved problem for some low diffusion schemes when simulating the hypersonic flow. In this paper, a simple method is proposed to enhance the robustness of the low diffusion schemes to overcome the shock anomaly. The main idea of this method is adding an appropriate extra term to the original low diffusion schemes without influencing the accuracy in aerodynamic heating prediction. This extra term is derived from the difference between the flux splitting scheme (FVS) and the advection upstream splitting method+ (AUSM+). Adding this term to three low diffusion schemes, seven typical numerical tests are conducted to examine the capability of those schemes. Numerical results show that the three new schemes turn out to be carbuncle-free and shock-stable without losing their original accuracy in prediction of aerodynamic heating, validating the feasibility and reliability of the proposed method.

1. Introduction

Over the years, the numerical schemes to calculate the inviscid fluxes of Euler/Navier-Stokes (N-S) equations in compressible flow simulations have a great development. In the early years of 1960s–1970s, the central schemes were commonly used [1]. But those schemes have some disadvantages such as poor accuracy in resolving intermediate characteristic fields and free parameters which are dependent on the problems [2]. In the late 1970s, the upwind schemes were introduced. The upwind schemes have many advantages such as a good robustness and being consistent with the physical characteristic. Nowadays, the widely used upwind methods include flux vector splitting (FVS), flux difference splitting (FDS) and AUSM (advection upwind slitting method)-type scheme. FVS is considered to be a natural consequence of the idea that regards a fluid as an ensemble of particles [3]. At the interface, some particles will move forward, others backward. The inviscid fluxes are automatically split into forward and backward fluxes. Actually, this kind of splitting method can be obtained by splitting the eigenvalue matrix of the Jacobian matrix. Different FVS schemes such as Steger-Warming (SWS) and Van Leer (VLS) have been presented according to different splitting implementations. Because of the capability of capturing the shock accurately and robustly, FVS had been very popular during the Euler era [3]. But this scheme has a poor accuracy in the boundary layer region which is attributed to its nature of excessive numerical diffusion. So it is an undesirable scheme for solving the N-S equations. According to Godunov's idea of regarding the compressible flow problem between two adjacent grid cells as a local Riemann problem [4], the FDS schemes such as Roe's FDS [5], HLL and HLLE were proposed. In these schemes, either an exact or approximate solution of Riemann's problem is used to compute the numerical fluxes at cell interface. It is reported that these schemes can provide the accurate solution on capturing the discontinuities. For the N-S solver, the FDS schemes have the good performance on resolving the boundary layer owing to its low numerical diffusion. However, the efficiency of FDS is inferior to that of FVS. AUSM which combines the efficiency of FVS and the accuracy of FDS was proposed in 1991 [6]. In this method, the cell-face advection Mach number is used to determine the upwind direction of the convective quantities. The pressure at the interface is calculated by summing two pressure splitting terms. It is reported that AUSM has low numerical diffusivity [7]. This simple and accurate scheme was very popular and attracted lots of attention. Several similar schemes were then proposed to improve the AUSM such as AUSM+ [8] and AUSMPW+ [9].

As mentioned above, enormous advances have been obtained during the last forty years. It seems that the numerical flux schemes are almost mature. However, as pointed out by some researchers [1,10,11], in order to get a better numerical solution of the entire computation domain for hypersonic numerical simulations, the two basic problems are still remained [10,11], i.e., the boundary-layer resolution and the robustness against shock anomalies. In this paper focus will be put on the shock anomaly

* Corresponding author.
E-mail address: wqtao@mail.xjtu.edu.cn (W.-Q. Tao).

Nomenclature

a	acoustic speed, m/s
E	total energy, J/kg
H	enthalpy, J/kg
M	Mach number
p	pressure, Pa
t	time, s
T	temperature, K
u	velocity in x-direction, m/s
v	velocity in y-direction, m/s
x	Cartesian coordinate, m
y	Cartesian coordinate, m

Greek symbols

β	correction factor
ϵ	correction factor
γ	specific heat ratio
λ	thermal conductivity, $Wm^{-1}K^{-1}$
μ	dynamic viscosity, $Pa \cdot s$
ρ	density, kg/m^3
τ	stress tensor

Subscripts

L	left
R	right
$1/2$	interface
∞	freestream

problem. A common shock anomaly is the carbuncle phenomenon. In 1988, Peery and Imlay [12] used Roe's FDS to study the hypersonic flow over a blunt body and found some abnormal bow shock solutions before the stagnation point. They firstly named it as carbuncle phenomenon. There are also some other shock anomalies such as kinked Mach stem found in double Mach reflection problem and odd-even decoupling solution in Quirk's test [13]. It is reported that the low numerical diffusion schemes such as Roe's FDS, AUSM+ and AUSMPW+ usually suffer from the shock anomalies [14]. Although the FVS schemes are free from the shock anomalies because of the good robustness, but they have the problem of poor accuracy of resolving the boundary-layer.

There have been lots of studies about the shock anomalies. Pandolfi and D'Ambrosio analyzed some significant aspects of the carbuncle phenomenon [15]. It is observed that grid aspect ratio is a very important factor on initiating the carbuncle phenomenon. The spindly grid cells along the normal direction of the shock usually promote the anomalies. It is also reported that this phenomenon often appears when first-order accuracy in space is used. Liou studied the numerical diffusivity of several outstanding upwind schemes and proposed a conjecture that if the mass flux of the upwind scheme did not rely on the pressure term, the scheme would be free from carbuncle phenomenon [16]. However, some counterexamples of this conjecture [17] indicate that Liou's conjecture may not be suitable for all the schemes. Xu studied the physical reason of shock instability and came to a conclusion that the shock anomalies did not occur on unstructured grid [18]. But this is contrary to the study of Ramalho et al. [19]. Sanders et al. analyzed the shock instability in strictly upwind finite difference schemes and proposed a possible method to cure the carbuncle solution [20]. But it is reported that this method has some problems in resolving the boundary-layer [15]. The rotated method and multidimensional hybrid method were proposed to cure the carbuncle phenomenon in [21–23]. But some problems still exist according to the research results of [24]. Some other different methods to cure the carbuncle phenomenon have been proposed [15,25,26]. But, they are later proved to be none universally effective [27].

From the above brief review, it seems that the reasons of causing the shock anomalies are still not very clear [28] and the methods to cure the anomalies proposed are case dependent. It is well-known that the cures of the shock anomalies are very important for simulating the hypersonic flows accurately. Thus, this problem should be further studied. Recently, there are some new methods published to reduce the shock anomalies [28–32]. In summary, one new method should have the capability of reducing the shock anomalies and resolving the boundary-layer. In this paper, such a new method is proposed in the finite volume framework. The major idea of this method is adding an extra term to a low-diffusion scheme such that the original scheme turns to be a more dissipative but shock-robust FVS near a shock wave. Applying this method to schemes of Roe's FDS, AUSM+, and AUSMPW+, some numerical tests are studied. The results show that this simple method can enhance the robustness of those schemes without influencing the accuracy in the prediction of aerodynamic heating.

In the following, the governing equations of the compressible flow will first be briefly presented, followed by the detailed description of the proposed method. Then some numerical examples will be provided, including one-dimensional Riemann problems, two-dimensional Riemann problem, double Mach reflection problem, odd-even problem, inviscid flow over a cylinder, compressible laminar flow over a flat plate, and viscous flow over a cylinder. In the numerical solutions of all these problems, the proposed method shows its wide applicability. Finally, some conclusions are made.

2. Governing equations

The compressible N-S equations in two-dimensional space can be written as:

$$\frac{\partial \mathbf{U}}{\partial t} + \frac{\partial \mathbf{F}_1}{\partial x} + \frac{\partial \mathbf{F}_2}{\partial y} = \frac{\partial \mathbf{F}_{v1}}{\partial x} + \frac{\partial \mathbf{F}_{v2}}{\partial y} \tag{1}$$

where $\mathbf{U}$ and $\mathbf{F}_1, \mathbf{F}_2$ are the conservative variables and the inviscid fluxes, respectively. They are given by

$$\mathbf{U} = \begin{bmatrix} \rho \\ \rho u \\ \rho v \\ \rho E \end{bmatrix}, \quad \mathbf{F}_1 = \begin{bmatrix} \rho u \\ \rho u^2 + p \\ \rho vu \\ \rho H u \end{bmatrix}, \quad \mathbf{F}_2 = \begin{bmatrix} \rho v \\ \rho uv \\ \rho v^2 + p \\ \rho H v \end{bmatrix} \tag{2}$$

Here, ρ is the density. u, v are the components of velocity in x, y direction. E is the total energy. p is the pressure which can be calculated as:

$$p = (\gamma - 1)\rho[E - (u^2 + v^2)/2] \tag{3}$$

The enthalpy H is given as $H = \frac{\gamma}{\gamma-1} p/\rho + (u^2 + v^2)/2$. The viscous fluxes $\mathbf{F}_{v1}$ and $\mathbf{F}_{v2}$ are

$$\mathbf{F}_{v1} = \begin{bmatrix} 0 \\ \tau_{xx} \\ \tau_{xy} \\ u\tau_{xx} + v\tau_{xy} + \lambda \frac{\partial T}{\partial x} \end{bmatrix}, \quad \mathbf{F}_{v2} = \begin{bmatrix} 0 \\ \tau_{yx} \\ \tau_{yy} \\ u\tau_{yx} + v\tau_{yy} + \lambda \frac{\partial T}{\partial y} \end{bmatrix} \tag{4}$$

Here, τ is the stress tensor of the fluid. T is the temperature. The dynamic viscosity of air μ is obtained by the Sutherland formula. The thermal conductivity of air is calculated as $\lambda = c_p \mu / Pr$. For a calorically perfect gas, $\gamma = 1.4$ and the Prandtl number Pr is taken as 0.72.

3. The method of improving the low diffusion schemes

As mentioned in the introduction, most of the low diffusion shock-capturing schemes suffer from the problem of shock anoma-

lies. In order to against the shock anomalies without losing the accuracy in the boundary-layer, one of the ideas is keeping the capability of FVS on simulating the shock wave while holding the low diffusion property in the boundary-layer. Following this idea, we proposed a method of adding an extra term to the original low diffusion schemes to increase the robustness without losing the accuracy in the boundary-layer region. In the finite volume method, the extra term of the inviscid fluxes at the cell interface is given as:

$$\mathbf{F}_{add} = \beta\epsilon^{3/2} a_{1/2}[M_L^+(\mathbf{\Phi}_L - \mathbf{\Phi}_{1/2}) + M_R^-(\mathbf{\Phi}_R - \mathbf{\Phi}_{1/2})] \tag{5}$$

Here, β and ϵ are the correction factors. The Mach number at the left and right side of the cell interface $M_{L/R}$ and the sound speed at the cell interface $a_{1/2}$ are calculated as follows [9]

$$\begin{aligned} &M_{L/R} = \tfrac{(u_n)_{L/R}}{a_{1/2}},\ \ a_{1/2} = \min(a_L, a_R) \\ &a = (a^*)^2/\max(|u_n|, a^*),\ \ a^* = \sqrt{2\tfrac{\gamma-1}{\gamma+1}H} \end{aligned} \tag{6}$$

$\mathbf{\Phi} = [\rho, \rho u_n, \rho u_\tau, \rho H]^T$. u_n and u_τ are the velocity in normal direction and tangential direction, respectively. $\mathbf{\Phi}_{1/2}$ is calculated according to the Mach number at the cell interface $M_{1/2}$ as

$$\mathbf{\Phi}_{1/2} = \begin{cases} \mathbf{\Phi}_L & M_{1/2} \geq 0 \\ \mathbf{\Phi}_R & M_{1/2} < 0 \end{cases} \tag{7}$$

$M^\pm$ is calculated as the one in reference [8]:

$$M^\pm = \begin{cases} \pm\dfrac{1}{4}(M \pm 1)^2 \pm \dfrac{1}{8}(M^2-1)^2 & |M| \leq 1 \\ \dfrac{1}{2}(M \pm |M|) & |M| > 1 \end{cases} \tag{8}$$

When calculating the inviscid fluxes at the cell interface, a new scheme can be obtained by adding $\mathbf{F}_{add}$ to the fluxes of the original low diffusion scheme as follows:

$$\mathbf{F}_{NEW} = \mathbf{F}_{original} + \mathbf{F}_{add} \tag{9}$$

In the following, the correction factors β and ϵ will be defined and discussed.

3.1. The correction factors

The region of the correction factors β and ϵ are both set to [0,1]. The first factor β is designed to meet the following conditions:

$$\begin{aligned} &\frac{\mathrm{d}\beta}{\mathrm{d}M_b} = C_0 M_b^3 (1 - M_b)^3 \\ &\beta(M_b = 0) = 0,\ \ \beta(M_b \geqslant 1) = 1 \end{aligned} \tag{10}$$

Here, C_0 is the constant. The local Mach number at the cell interface M_b and its component in i direction M_i are defined as:

$$M_{i=1} = \frac{|u_L + u_R|}{2a_{1/2}},\ \ M_{i=2} = \frac{|v_L + v_R|}{2a_{1/2}},\ \ M_b = \sqrt{M_1^2 + M_2^2} \tag{11}$$

By solving the above equations, the expression of β can be obtained as

$$\beta = \begin{cases} 35M_b^4 - 84M_b^5 + 70M_b^6 - 20M_b^7 & 0 \leq M_b \leq 1 \\ 1 & M_b > 1 \end{cases} \tag{12}$$

The variation of β with M_b is shown in Fig. 1.

The second correction factor ϵ is defined as

$$\epsilon = \begin{cases} \dfrac{1}{\max(N-1, 1)} \displaystyle\sum_{i=1}^{N} \left(1 - \frac{M_i}{M_b}\right)^2 & M_b \neq 0 \\ 0 & M_b = 0 \end{cases} \tag{13}$$

Here, N is the number of dimension. From the definition of ϵ, it can be seen that ϵ has the property of the variance in statistics. In two-dimensional situation, the larger the difference between M_1 and M_2, the greater the ϵ. For the situation of $M_b \neq 0$, the above equation can be simplified as

$$\epsilon(M_b \neq 0) = \begin{cases} 3 - 2\dfrac{M_1 + M_2}{M_b} & N = 2 \\ 0 & N = 1 \end{cases} \tag{14}$$

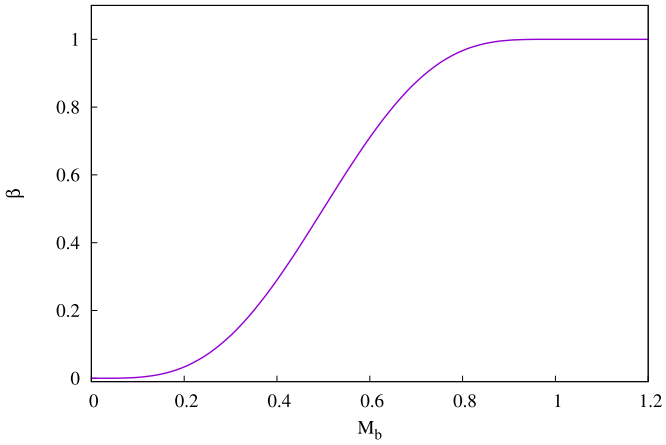

Fig. 1. The curve of β.

3.2. The analysis of the extra term

In 1995, Liou proposed the AUSM+ scheme to improve the AUSM [8]. It is reported that this scheme can resolve the boundary-layer and discontinuities exactly because of its low diffusion. In the AUSM+, the interface Mach number is used to decide the upwind direction. It is calculated as $M_{1/2} = M_L^+ + M_R^-$. In the scheme, the inviscid fluxes at the interface are calculated as [8]

$$\mathbf{F}_{AUSM+} = a_{1/2}(M_L^+ + M_R^-)\mathbf{\Phi}_{1/2} + P_L^+\mathbf{p}_L + P_R^-\mathbf{p}_R \tag{15}$$

On the other hand, one simple FVS can be rewritten as [33]

$$\mathbf{F}_{FVS} = a_L M_L^+ \mathbf{\Phi}_L + a_R M_R^- \mathbf{\Phi}_R + P_L^+\mathbf{p}_L + P_R^-\mathbf{p}_R \tag{16}$$

Here, the $M^\pm$ and $P^\pm$ have little differences with those used in Eq. (15).

Thus, compared with the above low diffusion scheme AUSM+, the extra diffusion of FVS can be expressed as

$$\begin{aligned} \mathbf{F}_{extra} &= \mathbf{F}_{FVS} - \mathbf{F}_{AUSM+} \\ &= a_{1/2}[M_L^+(\mathbf{\Phi}_L - \mathbf{\Phi}_{1/2}) + M_R^-(\mathbf{\Phi}_R - \mathbf{\Phi}_{1/2})] \end{aligned} \tag{17}$$

In the above equation, the differences between $a_{1/2}$, a_L, and a_R are neglected. Due to this extra diffusion, FVS is very robust on simulating the shock wave, while having the poor accuracy on resolving the boundary-layer.

Actually, this poor accuracy property of FVS can be easily demonstrated with the condition of $M_L = M_R = 0$. Under this zero-velocity condition, the inviscid fluxes at the interface should be $\mathbf{F}_{1/2} = \mathbf{p}_{1/2}$. However, the fluxes obtained by FVS can be written as:

$$\mathbf{F}_{1/2} = C(a_L\mathbf{\Phi}_L - a_R\mathbf{\Phi}_R) + \mathbf{p}_{1/2} \tag{18}$$

Here, the parameter C is not equal to zero. The value of C depends on which kind of FVS is used. For van Leer FVS, C is 0.25. Thus, the convective fluxes obtained by FVS are not necessarily equal to zero when $M_L = M_R = 0$. This property is obviously unsuitable for resolving the boundary-layer.

As mentioned above, our principle is enhancing the robustness without losing the accuracy of the scheme in the boundary-layer. This means that the extra diffusion term $\mathbf{F}_{extra}$ should be reduced

Table 1
Data of the 1-D Riemann problems.

Test	ρ_L	u_L	p_L	ρ_R	u_R	p_R	x_0	t_{end}
1	1.0	0.75	1.0	0.125	0.0	0.1	0.3	0.2
2	5.99924	19.5975	460.894	5.99242	−6.19633	46.095	0.4	0.035

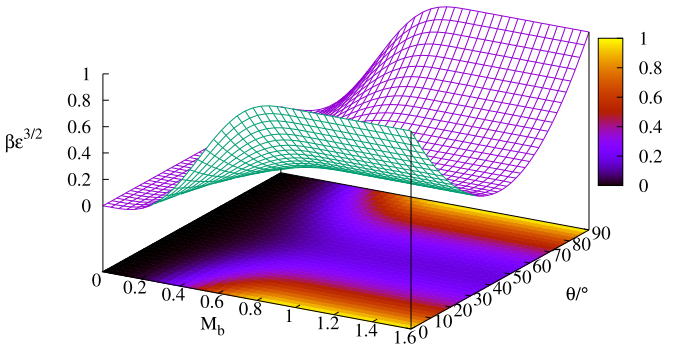

Fig. 2. The surface of $\beta\epsilon^{3/2}$.

in the boundary-layer region, especially when M_L and M_R are very close to zero. Therefore, the correction factor of β in Eq. (5) is introduced to let the influence of FVS be very small in the boundary-layer region. One simple form of β can be designed as a monotone increasing function with the conditions $\beta(M_b = 0) = 0$, $\beta(M_b \geqslant 1) = 1$. In addition, the following smooth increasing conditions are set to meet

$$\frac{d\beta}{dM_b}|_{M_b=0,1} = 0, \quad \frac{d^2\beta}{dM_b^2}|_{M_b=0,1} = 0 \tag{19}$$

Thus, Eq. (10) is implemented to determine the final form of β. As reported in the reference[15], shock anomaly often appears in the normal shock wave. The extra diffusion term $\mathbf{F}_{extra}$ can be further limited. The extra diffusion of enhancing the robustness only needs to be equal to $\mathbf{F}_{extra}$ near the normal shock region. It is well known that one of the features of a normal shock wave is that the difference between the velocity at the flow direction and the velocities at the other directions is large. Therefore, by referring to the idea of the variance in statistics, the second correction factor ϵ in Eq. (13) is adopted to assess the difference between the velocities at different directions.

In summary, the term $\beta\epsilon^{3/2}$ in Eq. (5) can be regarded as the switch function. Writing $M_1 = M_b\cos(\theta)$ and $M_2 = M_b\sin(\theta)$, the value of $\beta\epsilon^{3/2}$ can be obtained in Fig. 2. From the figure, it can be observed that $\beta\epsilon^{3/2}$ is quite small when M_b tends to zero. We have the relation $\beta\epsilon^{3/2}(M_b = 0) = 0$. Therefore, in the boundary-layer, the extra term $\mathbf{F}_{add}$ is small. It also can be found that $\beta\epsilon^{3/2}(\theta = 0^\circ, 90^\circ)$ is equal to 1 near the shock region. It means that the $\mathbf{F}_{add}$ is equal to the whole extra diffusion $\mathbf{F}_{extra}$ at this situation. The above analysis shows that the extra diffusion $\mathbf{F}_{extra}$ can be reduced in the boundary-layer by using the present extra term of Eq. (5).

4. Numerical experiments

As shown above, it is very easy to implement the present method in the finite volume framework. In this section, seven typical tests are simulated to examine the performance of three new schemes which are obtained by adding $\mathbf{F}_{add}$ to Roe's FDS, AUSM+, and AUSMPW+ respectively. These seven cases are:

1. 1D Riemann problems,
2. 2D Riemann problem,
3. $Ma_\infty = 10$ double Mach reflection,
4. $Ma_\infty = 6$ odd-even problem,
5. $Ma_\infty = 20$ inviscid flow over a cylinder,
6. $Ma_\infty = 0.8$ viscous flow over a flat plate,
7. $Ma_\infty = 6.47$ viscous flow over a cylinder.

In these simulations, the first five cases are used to assess the capability of the new schemes on capturing the discontinuities. The accuracy of the new schemes on resolving the boundary layer is evaluated in the final two cases.

4.1. One-dimensional Riemann problems

One dimensional Riemann problems are always used to test the capability of the numerical schemes on calculating different types of waves. Two typical one-dimensional tests are simulated. Following the simulations in reference [4], the first-order accuracy schemes in time and space are also used here. At the initial time, the flow field consists of two constant states $(\rho_L, u_L, p_L)^T$ and $(\rho_R, u_R, p_R)^T$. At the initial position $x = x_0$, the two constant states are separated by a discontinuity. The results are compared at the ending time $t = t_{end}$. The values of the above variables are given in Table 1. Here, we use the two-dimensional domain to simulate these one-dimensional problems. The correction factor ϵ is equal to 1. In these tests, the spatial domains are $x \in [0, 1] \times y \in [0, 10\Delta x]$. 100 grid points are used in x-direction ($\Delta x = 0.01$) with time step $\Delta t = 0.00025$.

Test 1 is a variant version of the famous Sod's test [4]. A right travelling shock wave, a contact wave and a left rarefaction wave exist in the solution. It is a very fundamental test. Test 2 is mainly designed to assess the ability of resolving slowly-moving contact discontinuities. The results of these two cases obtained by using different schemes are displayed in Figs. 3 and 4. It can be observed from the figures that there are nearly no differences between the results of the new schemes and the ones of the original schemes. Thus, in one-dimensional situation, the numerical results of different waves with different strength show that adding the present extra diffusion does not significantly influence the performance of the original schemes.

4.2. Two-dimensional Riemann problem

Compared with the above one-dimensional cases, the two-dimensional Riemann problem usually consists of a plethora of geometric wave patterns which cause some computational difficulties [34]. In this test, the computation domain is $x \in [0, 1] \times y \in [0, 1]$. 400×400 grid cells are used to discretize the domain. The time step Δt is 0.0001. A typical case is chosen in this test with the following initial flow field.

$$(p, \rho, u, v) = \begin{cases} (0.4, 0.5313, 0, 0) & x \in (0.5, 1], y \in (0.5, 1] \\ (1, 1, 0.7276, 0) & x \in [0, 0.5), y \in (0.5, 1] \\ (1, 0.8, 0, 0) & x \in [0, 0.5), y \in [0, 0.5) \\ (1, 1, 0, 0.7276) & x \in (0.5, 1], y \in [0, 0.5) \end{cases} \tag{20}$$

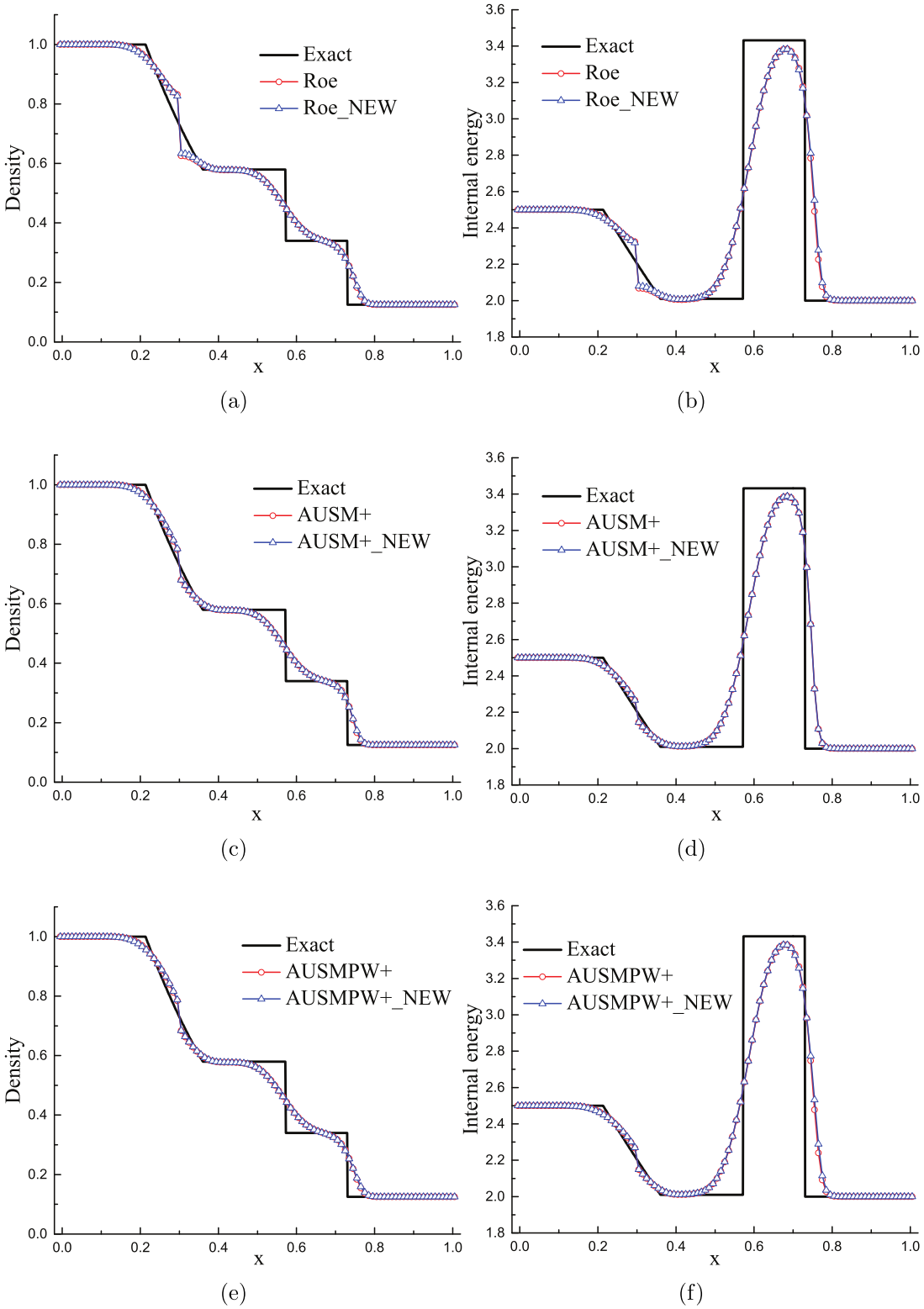

Fig. 3. Density and internal energy profiles for Test 1.

This simulation is implemented using the second-order accuracy scheme [35] with minmod limiter for spatial discretization and the second-order Runge-Kutta scheme for time-integration. At time $t = 0.25$, the results of the density field obtained by the three schemes and their revised versions are compared in Fig. 5. It can be found that the results of the original and new schemes have little differences. Adding the extra diffusion does not influence the accuracy of the original schemes. These results are very similar to those of [34].

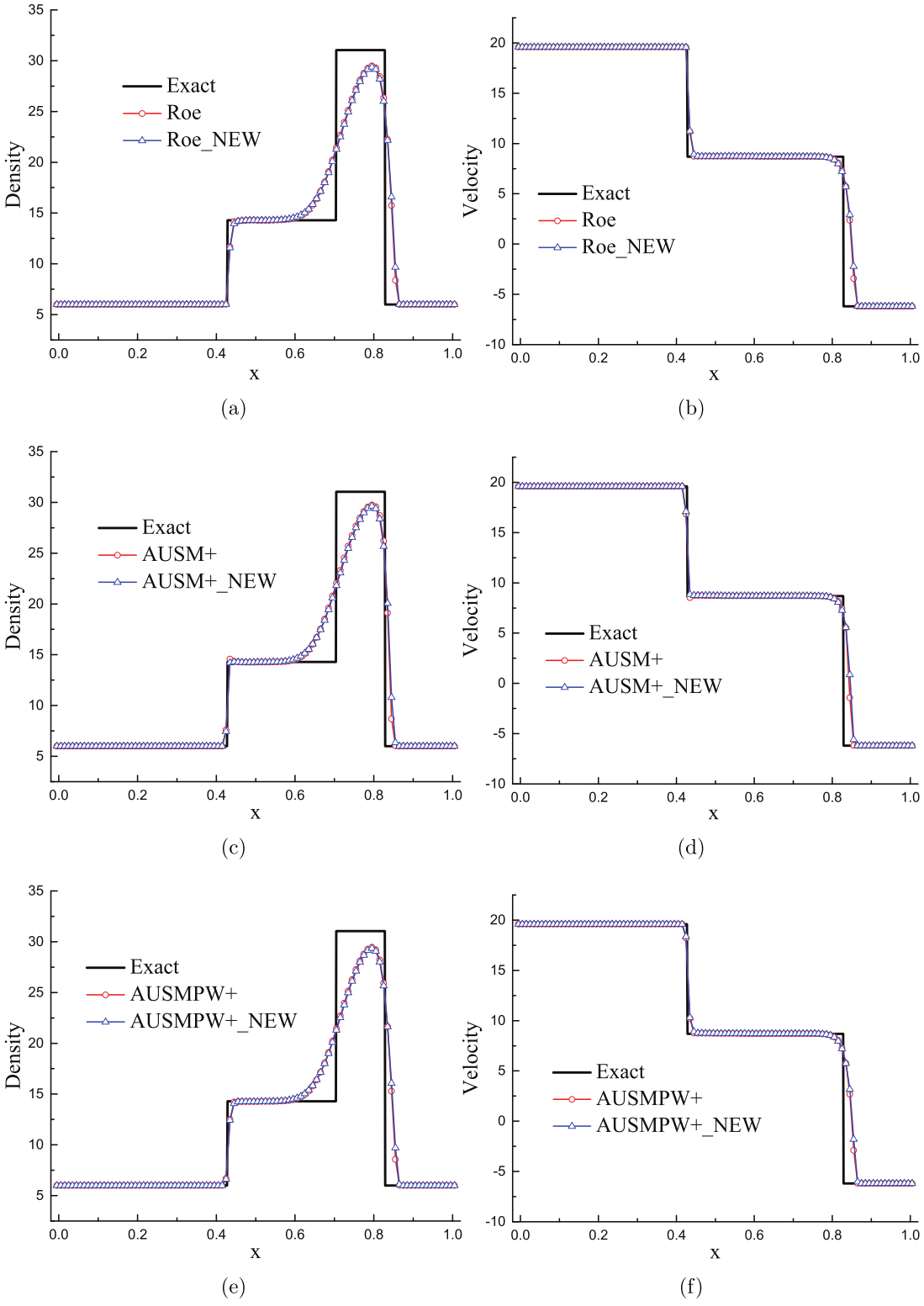

Fig. 4. Density and velocity profiles for Test 2.

4.3. Double Mach reflection problem

The double Mach reflection problem is usually used to check if one scheme can produce a nonphysical artifact which is caused by insufficient transverse dissipation. This nonphysical artifact usually appears as the kinked Mach stem when using lots of the low diffusion schemes to solve this problem. In this test, the spatial domain is $x \in [0, 4] \times y \in [0, 1]$. 400 × 400 grid cells are used in the simulation with the CFL number equals 0.5. At the initial time, a Mach 10 shock is set obliquely in the domain. The initial conditions are as follows:

$$(\rho, u, v, p) = \begin{cases} (8.0, 8.25\cos(30^\circ), \\ \quad -8.25\cos(30^\circ), 116.5) & x < \frac{1}{6} + \frac{y}{\sqrt{3}} \\ (1.4, 0.0, 1.0) & x \geq \frac{1}{6} + \frac{y}{\sqrt{3}} \end{cases} \tag{21}$$

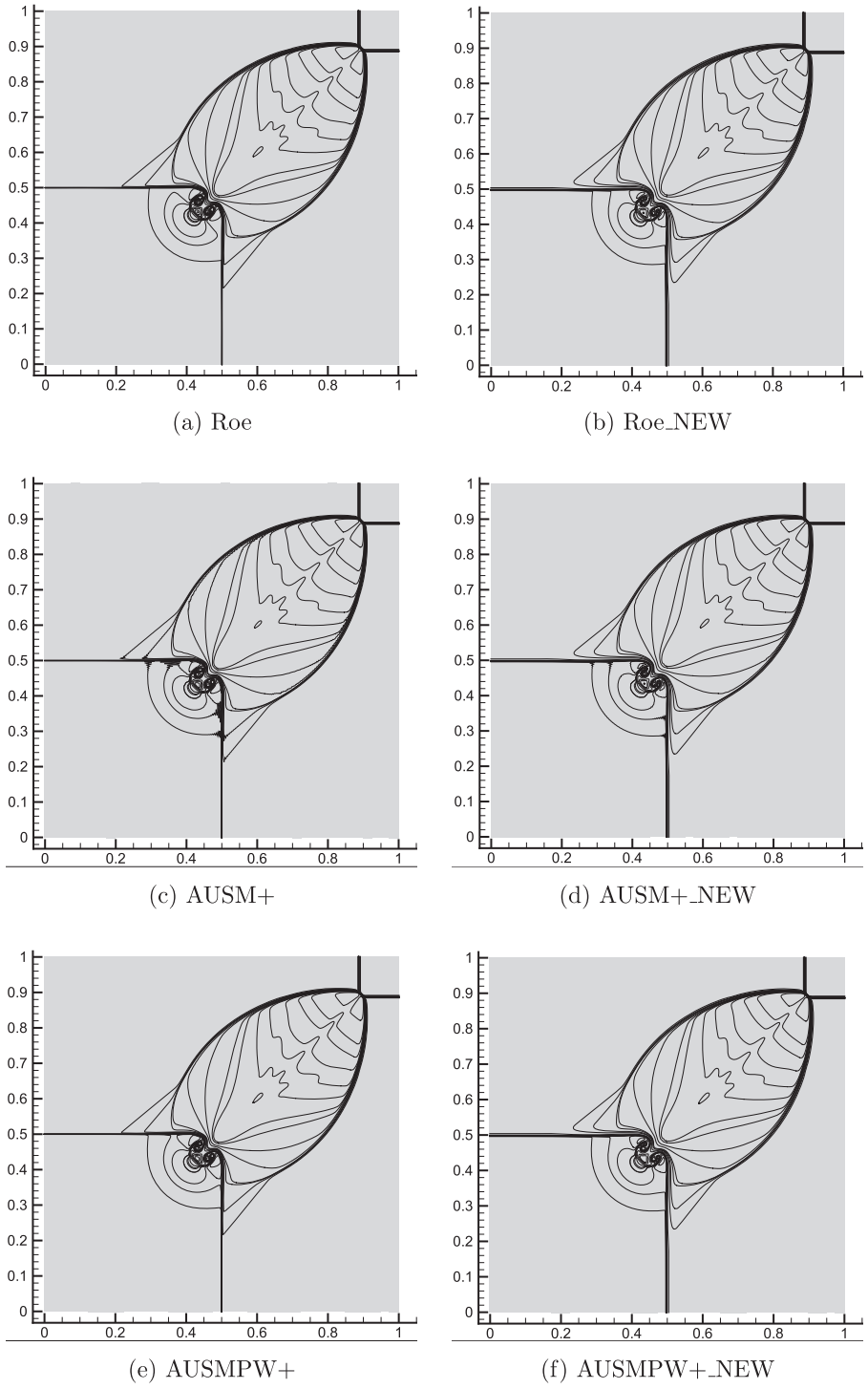

Fig. 5. Density contours of the 2-D Riemann problem.

The detailed information about this problem can be found in [36]. As mentioned in Section 1, the grid aspect ratio and first-order accuracy scheme in space are very important factors in initiating the shock anomalies. In order to critically validate the new schemes, a very large aspect ratio ($\Delta x/\Delta y = 4$) is used. In this test case and the following simulations about shock anomaly, the first-order accuracy schemes in space and time are adopted.

At time $t_{end} = 0.2$, the results obtained by the different schemes are compared in Fig. 6. From the density contours, it can be seen that Roe's FDS, AUSM+ and AUSMPW+ all produce the kinked Mach stem. By adding the present extra diffusion term, the results of these schemes are improved and such phenomenon does not exist. In this typical and severe test case, the results clearly demonstrate that the present extra diffusion term can significantly increase the robustness of the low diffusion schemes to eliminate the phenomenon of kinked Mach stem.

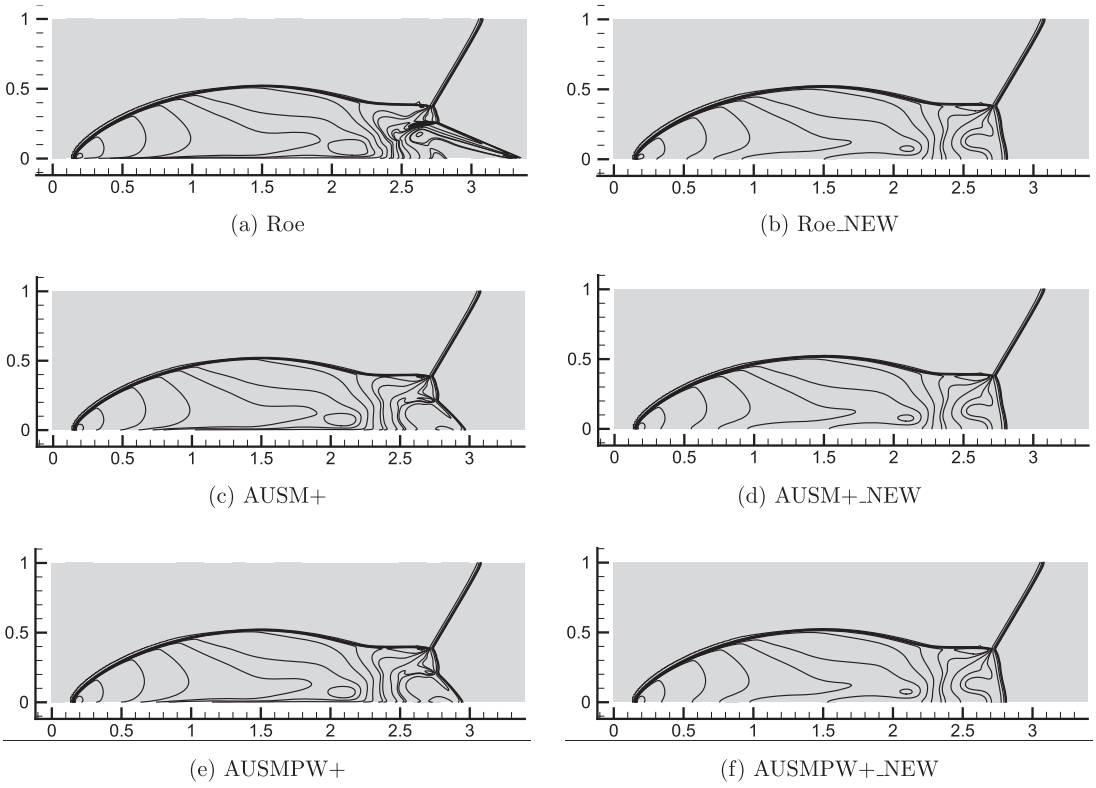

Fig. 6. Density contours of the double Mach reflection problem.

4.4. Odd-even problem

The odd-even problem which was first proposed by Quirk is usually used to examine whether a scheme is free from shock instability [13]. This test corresponds to the problem in which a Mach 6 planar shock moves from the left to the right in a duct. In our simulation, the computational domain is discretized by a structured grid with 800 × 20 cells. The size of each grid cell is $\Delta x = \Delta y = 1.25$. The CFL number is 0.5. At initial time, $\rho = 1.4, p = 1.0, u = 0, v = 0$. According to the Rankine-Hugoniot equations, the left boundary which can be regarded as the post-shock condition is $\rho = 7.376, p = 41.833, u = 4.861, v = 0$. The right boundary is zero gradient condition. The top and bottom boundary are both solid wall. In the simulation, some grid perturbations are introduced at center-line of the grid as follows [33]:

$$y_{i,j_{mid}} = y_{j_{mid}} + (-1)^i \times 10^{-n} \tag{22}$$

Here, i is the grid subscript in x-direction, n is taken as 2.

It is well-known that the small grid perturbations usually cause many upwind schemes to fail to simulate this simple problem. In this simulation, first order spatial accuracy is used. At time t = 150, the results of the density field obtained by different schemes are compared in Fig. 7. As shown in the figure, the shock instabilities can be found in the results of Roe's FDS, AUSM+ and AUSMPW+. On the contrary, their correspondent new schemes can perfectly simulate this problem because of the good robustness obtained by the present extra diffusion term.

4.5. $Ma_\infty = 20$ inviscid flow over a cylinder

As mentioned in the introduction, the carbuncle phenomenon was firstly named in the simulation of hypersonic flow over a blunt body. So this kind of problem is a typical one to check if a scheme can cause catastrophic carbuncle failings. The carbuncle phenomenon often means a spurious solution of the bow shock near the flow center line ahead of the blunt body. Here, the problem of Mach 20 flow over a cylinder is chosen to test these schemes. The radius of the cylinder is 1. The initial states are $\rho = 1.4, p = 1.0, u = 20, v = 0$. The computational domain is covered by 40×1020 (radial direction × circumferential direction) structured grid cells. The CFL number is 0.5.

Fig. 8 shows the results of density obtained by Roe's FDS, AUSM+, AUSMPW+, and their new schemes. It can be seen that the carbuncle phenomenon exists in the density contours of these original low diffusion schemes (Fig. 8(a), (c), (e)). Compared with the results of the corresponding original schemes, the results of those new schemes are greatly improved (Fig. 8(b), (d), (f)). In this test, the present extra diffusion term can indeed increase the robustness of Roe's FDS, AUSM+ and AUSMPW+.

4.6. $Ma_\infty = 0.8$ viscous flow over flat plate

When trying to enhance the robustness of the low diffusion schemes, one important principle is that the method should not affect the accuracy of the original schemes in resolving the boundary-layer region. As can be seen from the above tests, the present extra diffusion term can enhance the robustness of Roe's FDS, AUSM+ and AUSMPW+. In this part, the accuracy of those new schemes which are obtained by adding the extra diffusion in Eq. (5) is examined on the $Ma_\infty = 0.8$ laminar flow over a flat plate.

In this test case, the computational domain is $x \in [-0.25, 1] \times y \in [0, 0.25]$. On the bottom boundary, the no-slip and adiabatic boundary conditions are implemented in the region of $x \in [0, 1]$, while the other region is symmetric boundary conditions. The free stream parameters are $Ma_\infty = 0.8, T_\infty = 1/\gamma, \rho_\infty = 1.0, Pr =$

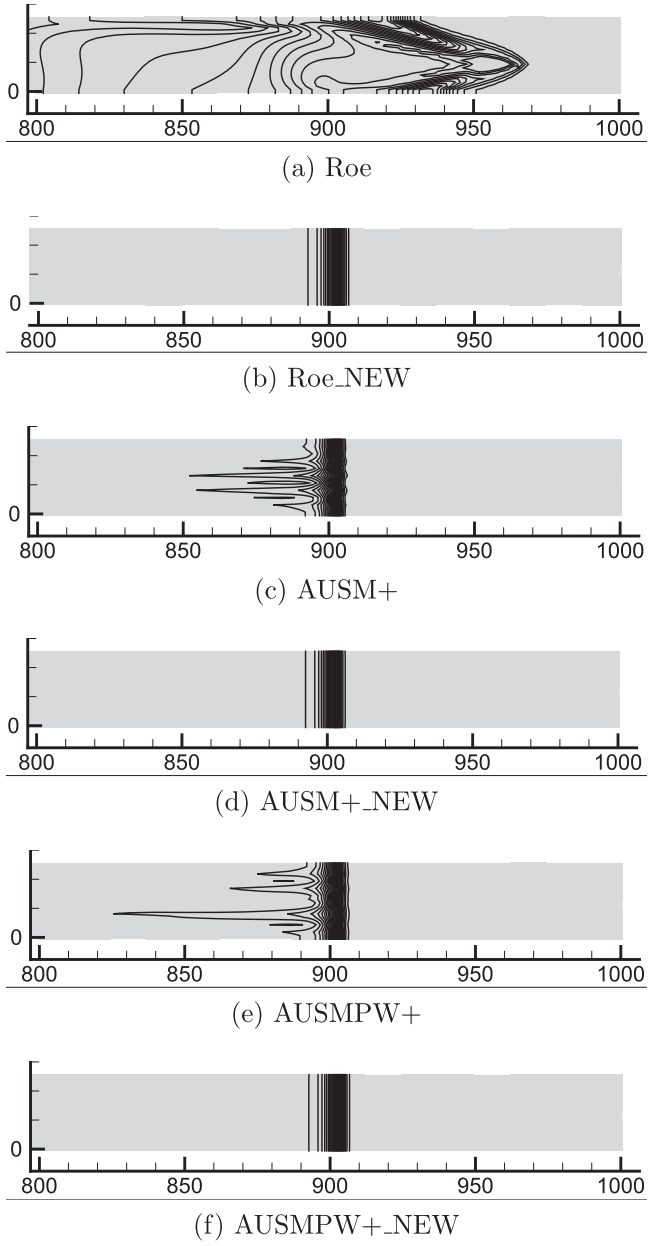

Fig. 7. Density contours of the odd-even problem.

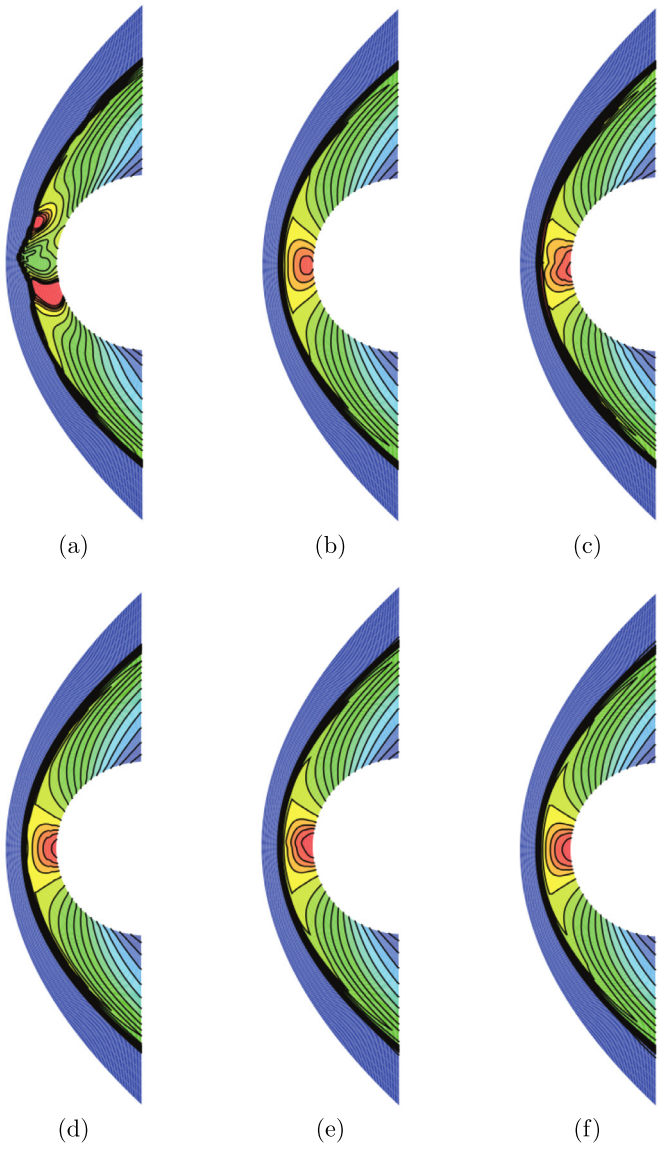

Fig. 8. Density contours of the Ma 20 inviscid flow. (a) Roe, (b) Roe_NEW, (c) AUSM+, (d) AUSM+_NEW, (e) AUSMPW+, (f) AUSMPW+_NEW.

1.0, $\gamma = 1.4$. The Reynolds number $Re_\infty = 5.0 \times 10^4$. The viscosity is set to meet the condition of $\rho\mu = \rho_\infty\mu_\infty$. 350×180 grid points are used in the simulation. The minimum grid size of Δy near the wall is 2.5×10^{-4}. The CFL number is set to 0.5. In this simulation and the following case of viscous flow, the numerical results are obtained by using the second-order centered scheme for the viscous fluxes, the third-order MUSCL scheme with minmod limiter [9] for the inviscid fluxes, and the third-order Runge-Kutta scheme for time-integration.

Fig. 9 shows the theoretical distributions of velocity and temperature and the distributions obtained by the different numerical schemes at $x = 0.8$. In the figure, η is the dimensionless coordinate with Illingworth transform [37]. The analytical solution of temperature profile for compressible flow over flat plate is given by White and Corfield [37]

$$\frac{T}{T_e} = 1 + \frac{\gamma - 1}{2} Ma_e \left(1 - \frac{u^2}{U_e^2}\right) \tag{23}$$

Here, T_e, U_e, Ma_e are the temperature, velocity, and Mach number at the outer edge, respectively. It can be observed from the figure that the results of the new schemes and the ones of the original schemes are matched very well. The accuracy of the original schemes on resolving the boundary-layer is not contaminated by the extra term.

4.7. $Ma_\infty = 6.47$ *viscous flow over a cylinder*

Here, the viscous hypersonic flow over a cylinder is tested. The radius of the cylinder is 38.1mm. The free stream conditions are $Ma_\infty = 6.47, T_\infty = 241.52$ K, $P_\infty = 648.13$ Pa. The wall temperature is 294.4 K. In this simulation, a structured mesh with 100×60 (radial direction × circumferential direction) nodes is used with the CFL number is about 0.3.

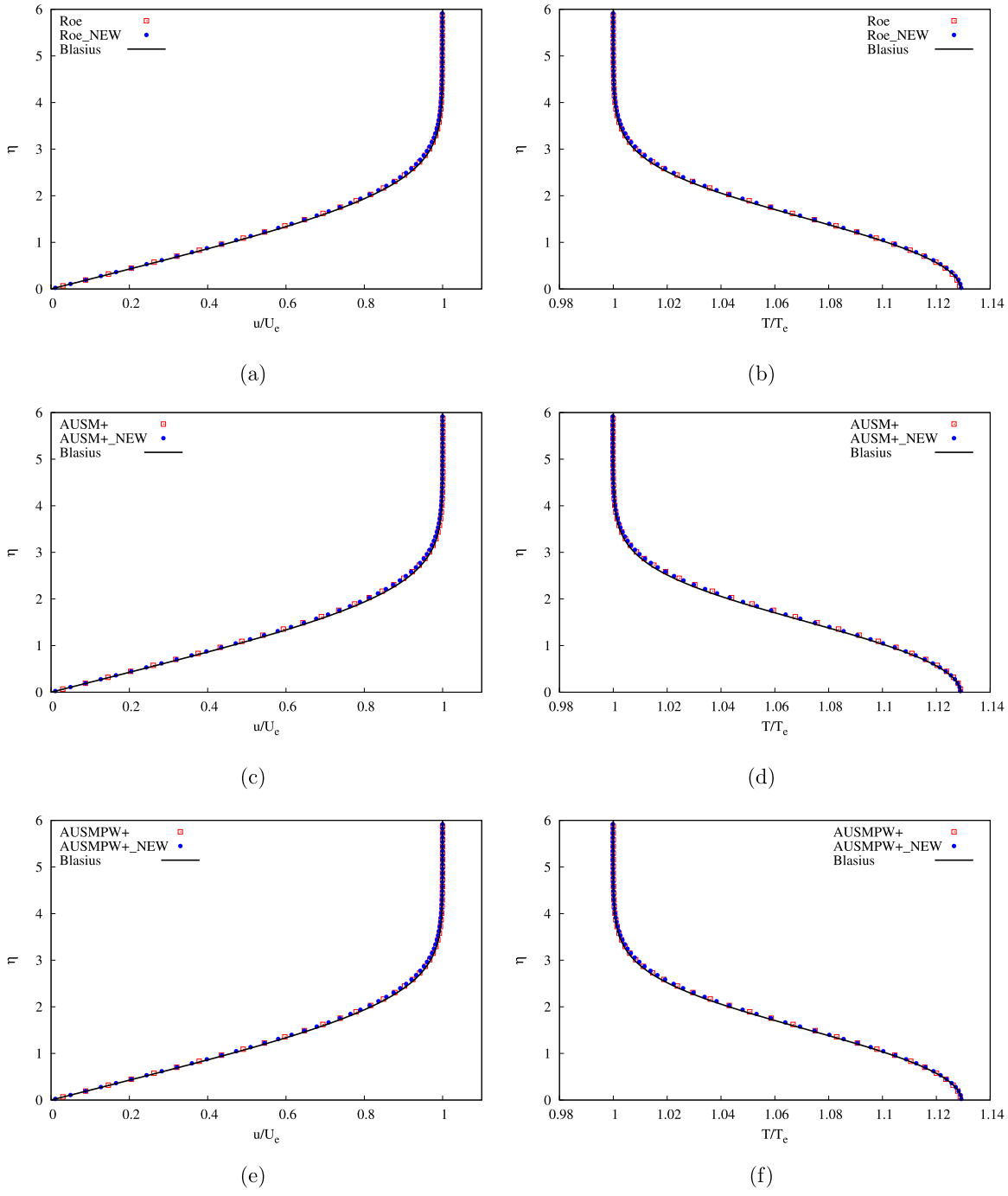

Fig. 9. Profiles of velocity and temperature at $x = 0.8$.

The wall heat fluxes and density contours are shown in Figs. 10 and 11, respectively. From Fig. 10, it can be observed that the wall heat fluxes obtained by those schemes are very close except for the results of Roe's FDS and van Leer FVS, which are obviously not correct. Fig. 11(a) shows the density contours obtained by Roe's FDS. It is very clear that this solution suffers from the carbuncle phenomenon. Because of this carbuncle failing, the wall heat fluxes predicted by Roe's FDS have a maximum deviation of 32.9% with the results of AUSMPW+, while the maximum deviation between the results of AUSMPW+ and Roe_NEW is 0.9%. Because of excess numerical diffusion, the wall heat fluxes obtained by van Leer FVS are very far from those of the low diffusion schemes (AUSM+, AUSMPW+). From this test case, it can be found that the extra term can enhance the robustness of low diffusion schemes without losing accuracy in the prediction of aerodynamic heating.

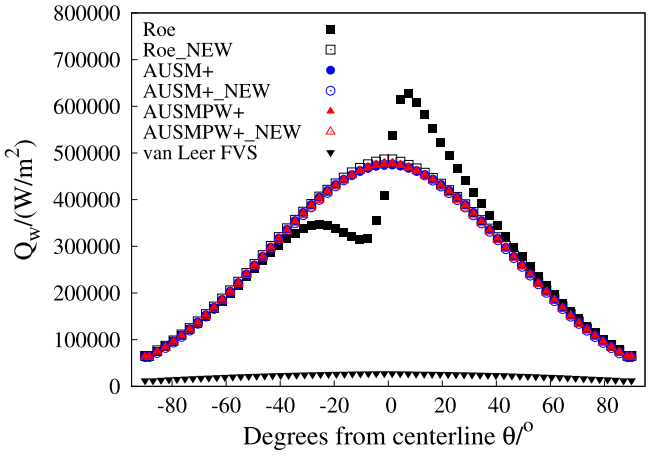

Fig. 10. The heat flux distributions on the solid wall.

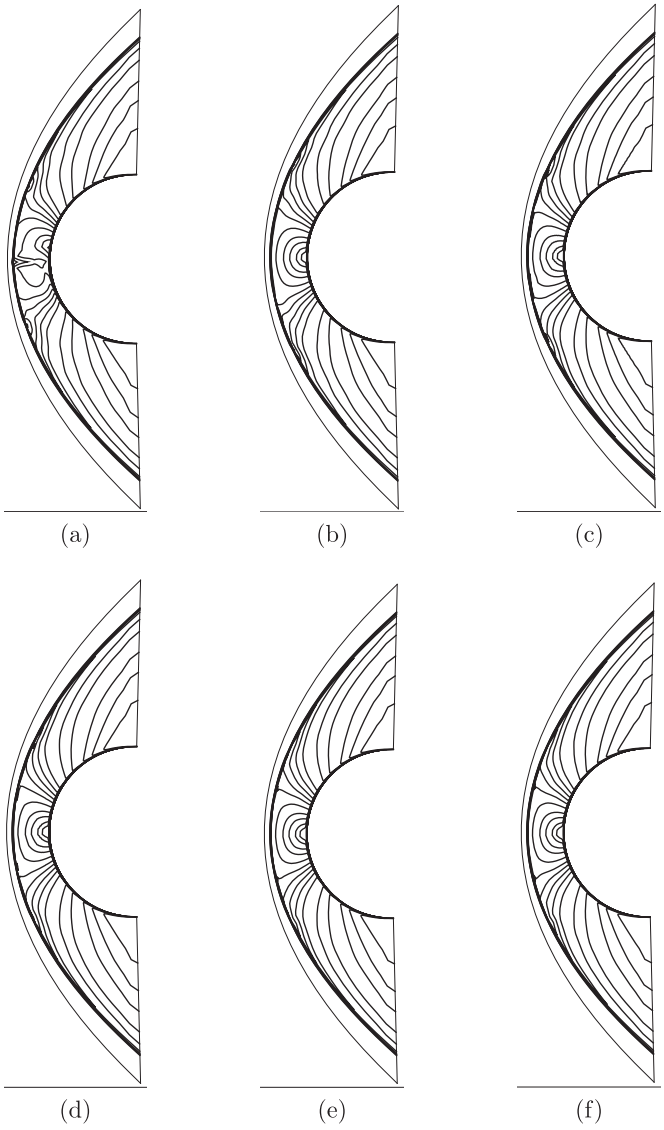

Fig. 11. Density contours of the Ma 6.47 viscous flow. (a) Roe, (b) Roe_NEW, (c) AUSM+, (d) AUSM+_NEW, (e) AUSMPW+, (f) AUSMPW+_NEW.

5. Conclusions

For enhancing the robustness of low diffusion schemes, a simple method is proposed in this paper. The idea of this method is to introduce an appropriate extra diffusion term into the schemes of calculating the inviscid fluxes of Euler/N-S equations. The appropriate extra diffusion is designed to meet the requirement of increasing the robustness of the low diffusion schemes without losing accuracy in the prediction of aerodynamic heating. The typical numerical tests show that using this method will not influence the capability of those original schemes (Roe, AUSM+, AUSMPW+) on capturing the discontinuities. On the other hand, this method can indeed enhance those schemes' robustness of capturing the shock. The viscous flow tests show that the accuracy of the low diffusion schemes on resolving the boundary layer is not significantly influenced by the present extra term.

The present method has been implemented in the context of air with a perfect gas equation of state (EOS). For the hypersonic flow past a re-entry vehicle, a real gas usually has to be considered. The extension of the present method on the complex EOS needs to be made in further study.

Declaration of Competing Interest

The authors declare that they have no known competing financial interests or personal relationships that could have appeared to influence the work reported in this paper.

CRediT authorship contribution statement

Shaolong Guo: Methodology, Validation, Writing - original draft. **Wen-Quan Tao:** Writing - review & editing, Supervision.

Acknowledgments

The present work was supported by the Foundation for Innovative Research Groups of the National Natural Science Foundation of China (No.51721004) and 111 Project (B16038).

References

[1] M.-S. Liou, Open issues in numerical fluxes: proposed resolutions, in: 20th AIAA Computational Fluid Dynamics Conference, 2011, p. 3055.
[2] F. Qu, C. Yan, J. Yu, D. Sun, A new flux splitting scheme for the euler equations, Comput. Fluids 102 (2014) 203–214.
[3] B. van Leer, Flux-Vector Splitting for the 1990s, Technical Report N91-21073, NASA, 1991.
[4] E.F. Toro, Riemann Solvers and Numerical Methods for Fluid Dynamics: A Practical Introduction, Springer Science & Business Media, 2013.
[5] P.L. Roe, Approximate Riemann solvers, parameter vectors, and difference schemes, J. Comput. Phys. 43 (2) (1981) 357–372.
[6] M.-S. Liou, C.J. Steffen, A New Flux Splitting Scheme, Technical Report TM-104404, NASA, 1991.
[7] M.-S. Liou, C.J. Steffen Jr, A new flux splitting scheme, J. Comput. Phys. 107 (1) (1993) 23–39.
[8] M.-S. Liou, A sequel to AUSM: AUSM+, J. Comput. Phys. 129 (2) (1996) 364–382.
[9] K.H. Kim, C. Kim, O.-H. Rho, Methods for the accurate computations of hypersonic flows: I. AUSMPW+ scheme, J. Comput. Phys. 174 (1) (2001) 38–80.
[10] K. Kitamura, E. Shima, Y. Nakamura, P.L. Roe, Evaluation of euler fluxes for hypersonic heating computations, AIAA J. 48 (4) (2010) 763–776.
[11] K. Kitamura, E. Shima, Towards shock-stable and accurate hypersonic heating computations: a new pressure flux for AUSM-family schemes, J. Comput. Phys. 245 (2013) 62–83.
[12] K. Peery, S. Imlay, Blunt-body flow simulations, in: 24th Joint Propulsion Conference, 1988, p. 2904.
[13] J.J. Quirk, A contribution to the great Riemann solver debate, Int. J. Numer. MethodsFluids 18 (1994) 555–574.
[14] K. Kitamura, P.L. Roe, F. Ismail, An evaluation of euler fluxes for hypersonic flow computations, AIAA Pap. 2007-4465 (2007).
[15] M. Pandolfi, D. D'Ambrosio, Numerical instabilities in upwind methods: analysis and cures for the "carbuncle" phenomenon, J. Comput. Phys. 166 (2) (2001) 271–301.

[16] M.-S. Liou, Mass flux schemes and connection to shock instability, J. Comput. Phys. 160 (2) (2000) 623–648.
[17] M. Dumbser, J.-M. Moschetta, J. Gressier, A matrix stability analysis of the carbuncle phenomenon, J. Comput. Phys. 197 (2) (2004) 647–670.
[18] K. Xu, Gas Evolution Dynamics in Godunov-Type Schemes and Analysis of Numerical Shock Instability, Technical Report 99-6, ICASE, 1999.
[19] M.V. Ramalho, J.H. Azevedo, J.L. Azevedo, Further investigation into the origin of the carbuncle phenomenon in aerodynamic simulations, in: 49th AIAA Aerospace Sciences Meeting including the New Horizons Forum and Aerospace Exposition, 2011, p. 1184.
[20] R. Sanders, E. Morano, M.-C. Druguet, Multidimensional dissipation for upwind schemes: stability and applications to gas dynamics, J. Comput. Phys. 145 (2) (1998) 511–537.
[21] Y.-X. Ren, A robust shock-capturing scheme based on rotated Riemann solvers, Comput Fluids 32 (10) (2003) 1379–1403.
[22] H. Nishikawa, K. Kitamura, Very simple, carbuncle-free, boundary-layer-resolving, rotated-hybrid Riemann solvers, J. Comput. Phys. 227 (4) (2008) 2560–2581.
[23] K. Huang, H. Wu, H. Yu, D. Yan, Cures for numerical shock instability in HLLC solver, Int. J. Numer. MethodsFluids 65 (9) (2011) 1026–1038.
[24] F. Zhang, J. Liu, B. Chen, W. Zhong, Evaluation of rotated upwind schemes for contact discontinuity and strong shock, Comput. Fluids 134 (2016) 11–22.
[25] H.-C. Lin, Dissipation additions to flux-difference splitting, J. Comput. Phys. 117 (1) (1995) 20–27.
[26] S.-s. Kim, C. Kim, O.-H. Rho, S.K. Hong, Cures for the shock instability: development of a shock-stable roe scheme, J. Comput. Phys. 185 (2) (2003) 342–374.
[27] F. Ismail, P.L. Roe, H. Nishikawa, A proposed cure to the carbuncle phenomenon, in: Fourth International Conference on Computational Fluid Dynamics, Ghent, Belgium, 2006.
[28] N. Fleischmann, S. Adami, X.Y. Hu, N.A. Adams, A low dissipation method to cure the grid-aligned shock instability, J. Comput. Phys. 401 (2020) 109004.
[29] S. Simon, J. Mandal, A simple cure for numerical shock instability in the HLLC Riemann solver, J. Comput. Phys. 378 (2019) 477–496.
[30] S.-s. Chen, C. Yan, K. Zhong, H.-c. Xue, E.-l. Li, A novel flux splitting scheme with robustness and low dissipation for hypersonic heating prediction, Int. J. Heat Mass Transf 127 (2018) 126–137.
[31] A.V. Rodionov, Artificial viscosity to cure the shock instability in high-order Godunov-type schemes, Comput. Fluids 190 (2019) 77–97.
[32] Z.-X. Gao, H.-C. Xue, Z.-C. Zhang, H.-P. Liu, C.-H. Lee, A hybrid numerical scheme for aeroheating computation of hypersonic reentry vehicles, Int. J. Heat Mass Transf. 116 (2018) 432–444.
[33] S. Guo, W.-Q. Tao, A hybrid flux splitting method for compressible flow, Numer. Heat Transf. Part B 73 (1) (2018) 33–47.
[34] A. Kurganov, E. Tadmor, Solution of two-dimensional Riemann problems for gas dynamics without Riemann problem solvers, Numer. Methods Partial DifferEqu 18 (5) (2002) 584–608.
[35] J. Blazek, Computational Fluid Dynamics: Principles and Applications, Butterworth-Heinemann, 2015.
[36] P. Woodward, P. Colella, The numerical simulation of two-dimensional fluid flow with strong shocks, J. Comput. Phys. 54 (1) (1984) 115–173.
[37] F.M. White, I. Corfield, Viscous Fluid Flow, vol. 3, McGraw-Hill New York, 2006.